Available online at www.sciencedirect.com
ScienceDirect
Trans. Nonferrous Met. Soc. China 34(2024) 1333−1346
Transactions of Nonferrous Metals Society of China
www.tnmsc.cn

Heterogeneous nucleation and dendritic growth of niobium under containerless electrostatic levitation

Yan-qiu WANG[1,2], Fu ZHENG[1], Xiao-xiao LU[1,2], Zhi-bin SUN[1,2]

1. National Space Science Center, Chinese Academy of Sciences, Beijing 100190, China;
2. University of the Chinese Academy of Sciences, Beijing 101499, China

Received 20 October 2022; accepted 5 May 2023

Abstract: With the containerless electrostatic levitation method, the undercooling level and nucleation solidification mechanism of niobium samples of 99.7% and 99.95% in purity were comprehensively studied. The classical nucleation theory was used to measure and calculate the thermophysical and thermodynamic characteristics associated with the nucleation and solidification procedure. The measurement results show that the maximum undercooling of experimental samples is 455.7 K, while the hyper cooling limit of the niobium is derived at 739 K. The most probable nucleation undercooling, pre-exponential factor, nucleation activation energy, solid/liquid interface free energy, and the critical nucleus radius are determined. The dendrite growth velocity has a powerful relationship with undercooling, and the dendritic growth velocity of liquid niobium reaches 42.1 m/s at the undercooling of 454 K. The effect of the anisotropy of surface energy is taken into account, and the forecast results display excellent consistency with the experimental ones.
Key words: liquid niobium; heterogeneous nucleation; dendritic growth; nucleation solidification mechanism; containerless electrostatic levitation

1 Introduction

The morphology of the dendritic array is determined by the velocity of dendritic growth, which has important research implications for the microstructure of metal and alloy materials [1−3]. Crystal nucleation is the fundamental step in the solidification process, and it has a significant impact on the phase composition and structural morphology of the material [4,5]. Undercooling promotes dendrite growth and crystal nucleation. Finding new materials with superior properties and researching the solidification process of materials is critical, and different undercooling conditions result in nucleation and dendrite growth with different physical principles [6−8]. Because both dendritic growth and crystal nucleation occur at the solid/liquid interface, the solid/liquid interface free energy is an essential material property to comprehend crystal nucleation [9,10].

Because containerless processing technology eliminates heterogeneous nucleation caused by the container wall, the containerless experimental apparatus can be used to obtain droplets with significant undercooling [11,12]. Containerless levitation techniques include acoustic, aeroacoustic, electromagnetic, and electrostatic levitation, which are used to investigate the nucleation solidification mechanism, discover metastable phase materials, and measure the thermophysical properties of materials [13−16]. In comparison to existing containerless levitation technologies, containerless electrostatic levitation (ESL) technology, which provides a vacuum environment free of impurity, gas flow, and electromagnetic disturbance, has

Corresponding author: Xiao-xiao LU, Tel: +86-18800126158, E-mail: luxiaoxiao940312@163.com;
Zhi-bin SUN, Tel: +86-13810195052, E-mail: zbsun@nssc.ac.cn
DOI: 10.1016/S1003-6326(24)66475-7

emerged as a new method for material preparation [17].

RHIM et al [18] from the Jet Propulsion Laboratory (JPL) created the initial set of electrostatic levitation experimental apparatus in 1993. Later, research on electrostatic levitation technology and material research was successfully carried out by PARADIS and RHIM [19] from Japan, HORNFECK et al [20] from Germany, and LEE et al [21] from South Korea. WANG et al [17] from the National Space Science Center, Chinese Academy of Sciences (CAS) created a containerless electrostatic levitation facility and conducted an extensive study on the thermophysical characteristics of typical refractory metals in 2015. The electrostatic levitation device was then created by ZOU et al [22] from Northwestern Polytechnical University, China, XUE et al [23] from the Technology and Engineering Center for Space Utilization, CAS, and ZHONG et al [24] from the Shanghai Institute of Ceramics, CAS. The thermo- physical properties and undercooling nucleation mechanism of typical refractory metals such as zirconium, niobium, titanium, palladium, molybdenum, nickel, tungsten, terbium, and tantalum were investigated through the ESL method [25−34].

As a typical refractory metal with a melting temperature of about 2741 K, niobium (Nb) is mainly used in the aerospace and automotive industries to strengthen alloys [35]. Niobium has a variety of applications in the nuclear industry because of its refractory properties and resistance to corrosion. Traditional methods also face the risk of contamination due to the high molten temperature, which makes it challenging to correctly assess the thermophysical characteristics of niobium. In previous studies, the ESL technique was used to examine certain properties of pure niobium. For example, ISHIKAWA et al [25] measured the density and viscosity, and PARADIS et al [35] measured the density, thermal expansion coefficient, and constant pressure heat capacity through an electrostatic levitation furnace.

The ESL approach to studying the thermo-physical and thermodynamic properties of pure niobium has the advantages of improving thermo-physical property measurement accuracy, better understanding thermodynamic properties of niobium, and establishing the foundation for studying the thermophysical and thermodynamic properties of niobium-related alloys.

The diameter of the experimental samples used in this work is (2±0.02) mm, and the research objects are Nb with purity levels of 99.7% and 99.95%. The primary goal of this work is to reveal the characteristics of heterogeneous nucleation and solidification mechanisms, as well as the dendritic growth of Nb with varying degrees of purity using the ESL method. Previous studies reported little on the thermophysical and thermodynamic properties of liquid Nb with various impurities based on abundant experimental statistical analysis data. By combining theoretical research and experimental validation, our results are of great importance for the non-stationary solidification of metallic materials under deep undercooling conditions.

2 Experimental

The ESL experimental platform is composed of a vacuum chamber and peripheral measuring instruments. As shown in Fig. 1, the experimental

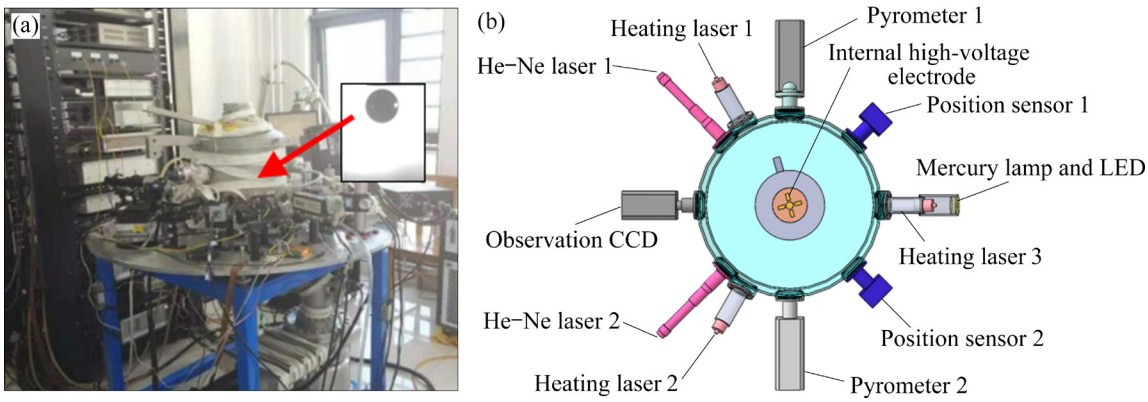

Fig. 1 Electrostatic levitation experiment device: (a) Diagram of overall experimental device; (b) Schematic diagram of top view of experimental platform and equipment

vacuum chamber is installed in the center of the horizontal experimental platform, and the measuring instruments are installed around the vacuum chamber. The upper and lower high-voltage electrodes are horizontally installed at the central axis in the vacuum chamber. The dynamic levitation of charged samples is realized by controlling the electric field intensity between the upper and lower electrodes. In the heating procedure, the temperature of the sample is measured in a real-time way with a pyrometer (Sensortherm H322), and the temperature measurement error is ±0.3%. Three 915 nm near-infrared semiconductor heating lasers (RFL-FDDL50X) are used to heat the sample, with a 120° included angle to each other. To realize the closed-loop control of sample temperature, the heating laser power is controlled by proportional-integral-derivative (PID) controller. The control frequency of sample temperature is 1000 Hz and the temperature control accuracy is ±5 °C. To reduce the influence of charge loss on sample position control during the heating process, a 500 W mercury lamp is used to irradiate the sample surface through a 200−400 nm ultraviolet filter. The lost charge of the sample is supplemented by the photoelectric effect so that the levitation position accuracy of the sample could reach ±0.1 mm. The sample will produce intense radiation in the high-temperature phase, which will affect the clarity of image edge of sample [32]. Therefore, it is necessary to place a backlight light-emitting diode (LED) as the light source to observe and obtain the levitation state images of the sample. Figure 1 shows the overall diagram of ESL in this work.

Prior to conducting the heating experiment, the vacuum level in the chamber is maintained at 10^{-5} Pa to prevent high-voltage electrode breakdown discharge and sample oxidation. The sample is positioned in the middle of the lower electrode at the start of the experiment. The sample is next preheated to 1500 K using a heating laser in order to prevent the occurrence of charge loss and to make sure that the thermionic emission regime effect is in the dominant role [33]. The material sample is then lifted to the center of the electrode by adjusting the strength of the electric field between the upper and lower electrodes. The sample is then heated to an overheated temperature by increasing the power of three heating lasers. Finally, the heating laser is turned off to make the sample turn into an undercooled state by natural radiation. When the temperature of the experimental droplet drops to the lowest undercooling temperature, the recalescence phenomenon occurs. After the sample is solidified completely, the heating laser was turned on again and the process of heating−melting−overheating−natural radiation cooling−undercooling−spontaneous nucleation−recalescence−natural cooling was repeated.

3 Results and discussion

3.1 Hypercooling limit of niobium

Under the electrostatic levitation condition, the temperature−time curves of niobium with different undercooling and the power change of the heating laser during the recalescence period are shown in Fig. 2.

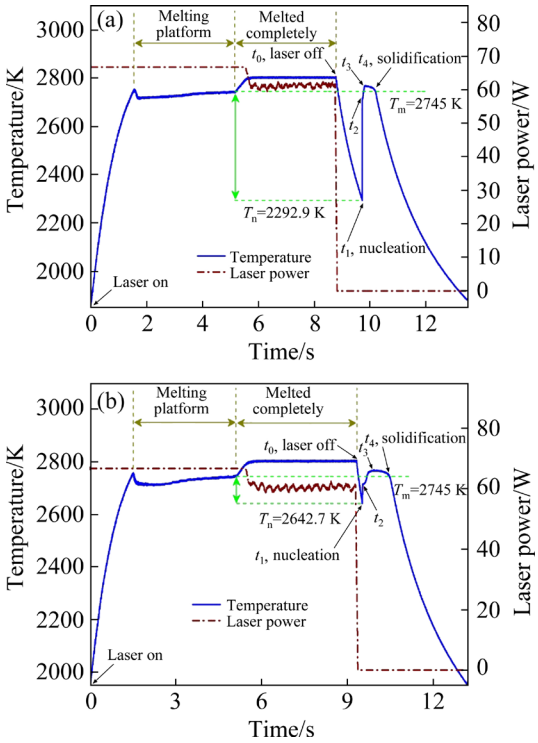

Fig. 2 Typical temperature−time curves and laser power changes for Nb sample under different undercoolings: (a) 452.1 K; (b) 102.3 K

During the heating process, when the sample temperature reaches the melting point T_m, a melting platform (a procedure for completely molten) will appear for a while. After the sample is completely melted, the sample temperature will continue to increase. At time t_0, the sample reaches the highest

temperature and the surface of the sample is approximately spherical due to surface tension. At this time, the heating laser is turned off, the sample is cooled by natural radiation, and the surface color of the sample changes from bright to dark. At time t_1, the sample temperature is cooled to T_n, and the nucleation point appears and grows rapidly. The difference value between T_n and T_m is undercooling (ΔT). At time t_2, due to the rapid release of crystallization latent heat, the temperature of the sample rises sharply to the melting point. The surface brightness increases suddenly, resulting in the recalescence phenomenon. The difference value between T_n and the sample temperature at t_2 is the recalescence degree (ΔT_r). Then, the residual liquid niobium solidifies slowly and the released latent heat reaches a balance with the heat dissipation, so the sample temperature maintains the melting point for a while, forming a solidification platform. The sample is completely solidified until t_4, and then it continues to cool by natural radiation. The period time from t_2 to t_4 is the solidification plateau time Δt_p.

The undercooled degree and solidification plateau time of the sample are obtained and analyzed from the temperature data. As shown in Fig. 3(a), with the increase of undercooling, the solidification plateau time decreases. If the undercooling of the droplet can increase to the hyper cooling limit, the solidification plateau time corresponding to slow solidification will disappear. Figures 3(b, c) show the relationship between undercooling ΔT (K) and solidification plateau time Δt_p (ms) of niobium with 99.7% and 99.95% purity, which satisfies the linear relationships: Δt_p=−1.442ΔT+1066.0 (99.7% Nb), and Δt_p=−1.436ΔT+1062.96 (99.95% Nb).

It can be deduced that when Δt_p is 0, the hyper cooling limit ΔT_h of niobium with 99.7% and 99.95% purity are 739.0 and 739.99 K, respectively. YANG et al [5] and KANG et al [9] measured the hypercooling limit of niobium through electrostatic levitation method, as given in Table 1. By differential scanning calorimeter and pulse heating technology, WILTHAN et al [34] measured the fusion enthalpy ΔH_m and specific heat capacity C_p of niobium are 33000 J/mol and 43.3 J/(mol·K), respectively. According to the equation ΔT_h=$\Delta H_m/C_p$, the hyper cooling limit of niobium can

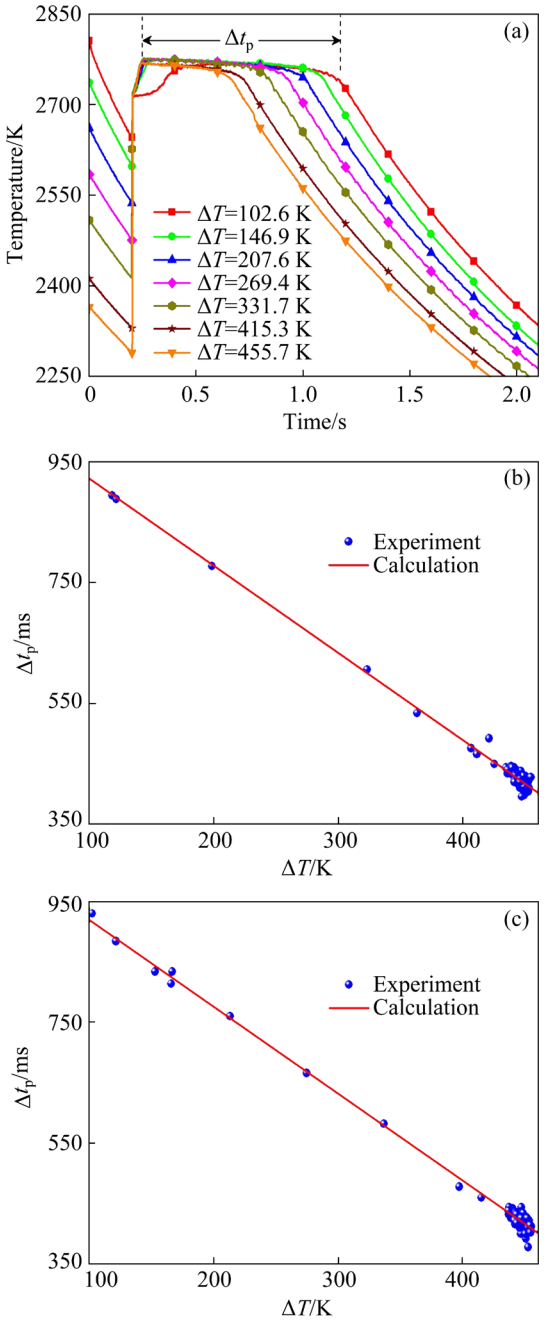

Fig. 3 Recalescence and solidification characteristics of Nb under ESL condition: (a) Temperature−time curves under different undercoolings; (b) Solidification plateau time versus undercooling of 99.7% Nb; (c) Solidification plateau time versus undercooling of 99.95% Nb

Table 1 Hypercooling limit of niobium

Source	Purity/%	ΔT_h/K	Remarks
This work	99.7	739.0	ESL
	99.95	739.99	ESL
YANG et al [5]	99.95	706	ESL
KANG et al [9]	99.95	640	ESL
WILTHAN et al [34]	99.9	762.1	Pulse heating

be calculated as about 762.1 K. Our experimental result is close to that of WILTHAN et al [34] (the error is within 5%), and our result is 13.4% higher than that of KANG et al [9].

3.2 Relationship between cooling rate and undercooling

The sample is in a high vacuum environment with no contact with the container wall under the electrostatic levitation condition, so there is no influence of heat conduction or heat convection. The molten sample is cooled by natural heat radiation between the time t_0 and t_1 in Fig. 2, which is a pure radiative cooling procedure without manual adjustment. The cooling rate is determined according to the gradient of each cooling curve. The cooling curve can be fitted with Eq. (1):

$$T=a(t+b)^{-1/3}+c \tag{1}$$

where T is the temperature; t is the time; a, b, and c are fitting coefficients.

A typical temperature fitting result in this work is shown in Fig. 4, and the calculated cooling fitting curve is consistent with the experimental data well. According to the fitted cooling curve, the cooling rate (R_c) of the sample at different time in the undercooled state can be calculated. Figure 5 reveals the relationships between R_c and ΔT of niobium at the nucleation moment. The relationship between cooling rate and undercooling degree shows a dramatically negative correlation, that is, the higher the cooling rate is, the lower the undercooling degree will be obtained. The result provides a possibility to get a higher undercooling degree by controlling the cooling rate.

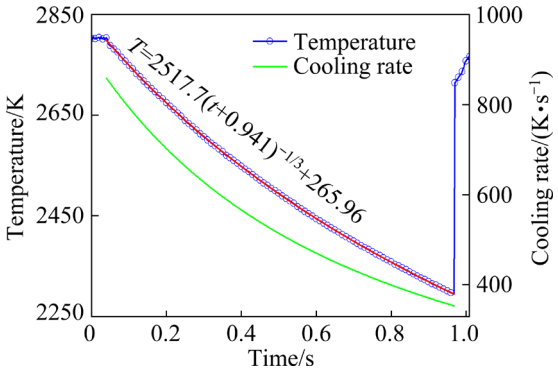

Fig. 4 Fitting cooling curve and cooling rate of undercooled Nb

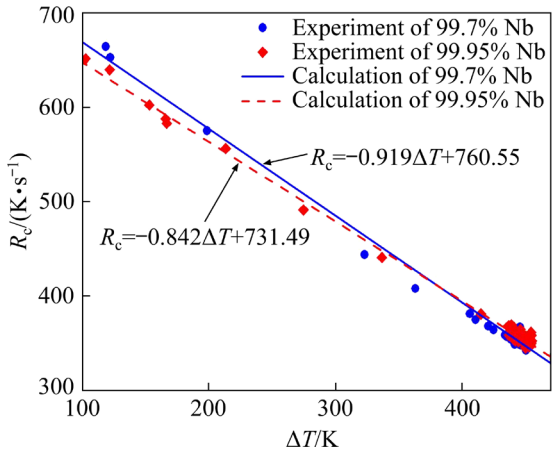

Fig. 5 Cooling rate versus undercooling at nucleation moment

3.3 Specific heat of undercooled niobium

The specific heat of metal liquid can be used to calculate other thermodynamic parameters, such as enthalpy, entropy, and Gibbs free energy, which are of special significance for the study of crystal metastable phase and solidification process. The ratio of C_p to emissivity ε_T of niobium is calculated by the following equation [25]. The ratio of C_p to ε_T is a physical parameter that reflects the radiation and heat dissipation capacity of materials:

$$\frac{C_p}{\varepsilon_T}=-\frac{A\sigma_0\,(T^4-T_a^4)(M/m)}{\mathrm{d}T/\mathrm{d}t} \tag{2}$$

where A is the sample surface area; σ_0 is the Stefan−Boltzmann constant; T is the sample temperature; T_a is the ambient temperature; M is the molar mass; m is the sample mass and $\mathrm{d}T/\mathrm{d}t$ is the cooling rate of the sample. The sample temperature is collected in real-time by the pyrometer and the cooling rate of the sample is obtained from the temperature fitting curve in Fig. 4. According to the relationship between the density ρ (kg/m^3) and undercooling ΔT (K) of liquid niobium measured by PARADIS et al [35]: ρ=7950+0.23ΔT, the surface area of the sample at different temperatures is calculated. Figure 6 demonstrates the ratio of C_p/ε_T on the temperature of liquid Nb, which is consistent with the following equation:

$$\begin{cases} C_p/\varepsilon_T=1.391\times10^{-5}T^2-0.0951T+296.94 \text{ (99.7\% Nb)} \\ C_p/\varepsilon_T=1.378\times10^{-5}T^2-0.0949T+296.47 \text{ (99.95\% Nb)} \end{cases}$$

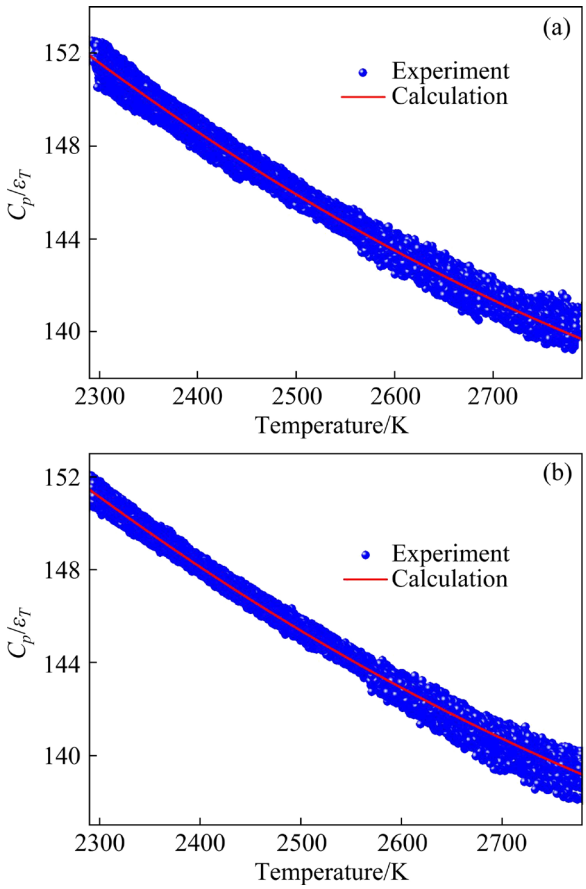

Fig. 6 Ratio of C_p/ε_T versus temperature of liquid Nb in deeply undercooled state: (a) 99.7% Nb; (b) 99.95% Nb

SAKATA et al [36] measured the emissivity of molten niobium at T_m as 0.29, by a blackbody radiation furnace. Usually, ε_T is assumed to not change with temperature in the liquid state, and the variation of C_p (J·mol^{-1}·K^{-1}) with T (K) of niobium in an undercooled state can be expressed as the following equation:

$$\begin{cases} C_p = 4.033\times10^{-6}T^2 - 0.0276T + \\ \quad 86.026 \text{ (99.7\% Nb)} \\ C_p = 3.998\times10^{-6}T^2 - 0.0275T + \\ \quad 85.978 \text{ (99.95\% Nb)} \end{cases} \tag{3}$$

According to the specific heat capacity at T_m and the hyper cooling limit, the fusion enthalpy ($\Delta H_m = C_p \cdot \Delta T_h$) of niobium with different purity is calculated in this work: ΔH_m=30112.23 J/mol (99.7% Nb) and ΔH_m=30013.72 J/mol (99.95% Nb).

The C_p values of niobium at the melting point of this work and other documents are listed in Table 2. The results are consistent with the measurement results of SAKATA et al [36], YANG et al [5], and BETZ and FRONHBERG [37] (the error is within 5%), and 6.78% lower than the measurement results of WILTHAN et al [34].

Table 2 Specific heat capacity of liquid niobium

Source	Purity/%	C_p at melting point/(J·mol^{-1}·K^{-1})	Remarks
This work	99.7	40.75	ESL
	99.95	40.55	ESL
SAKATA et al [36]	99.9	41.9	ESL
YANG et al [5]	99.95	41.5	ESL
BETZL and FRONHBERG [37]	99.96	40.6	Drop calorimetry
WILTHAN et al [34]	99.9	43.3	Pulse heating

3.4 Undercooling distribution and nucleation activation energy

According to previous research, nucleation is a probability event that complies with Poisson distribution in the undercooled state [5]. In this work, the heating and cooling experiments of 99.7% and 99.95% niobium materials are repeated 117 times and 126 times, respectively. The cumulative distributions of the two kinds of data are plotted in Fig. 7.

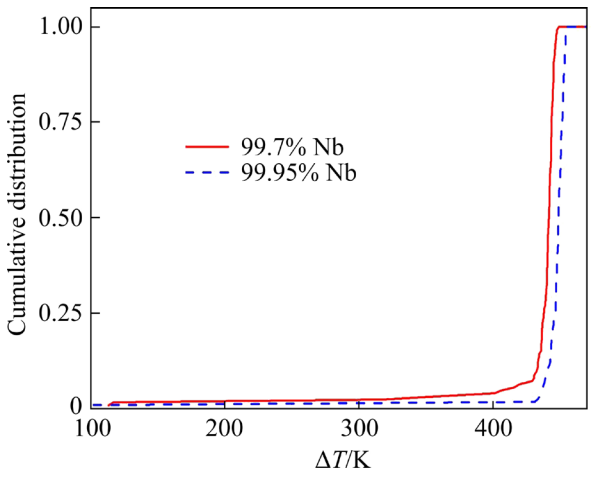

Fig. 7 Cumulative distributions of two kinds of niobium undercooling data

The probability density function of nucleation is counted, as shown in Fig. 8. It can be seen that for the niobium with 99.7% purity, the undercooling is mainly concentrated at 429−450 K, and the most probable nucleation undercooling is 442.7 K. For the niobium with 99.95% purity, the undercooling is

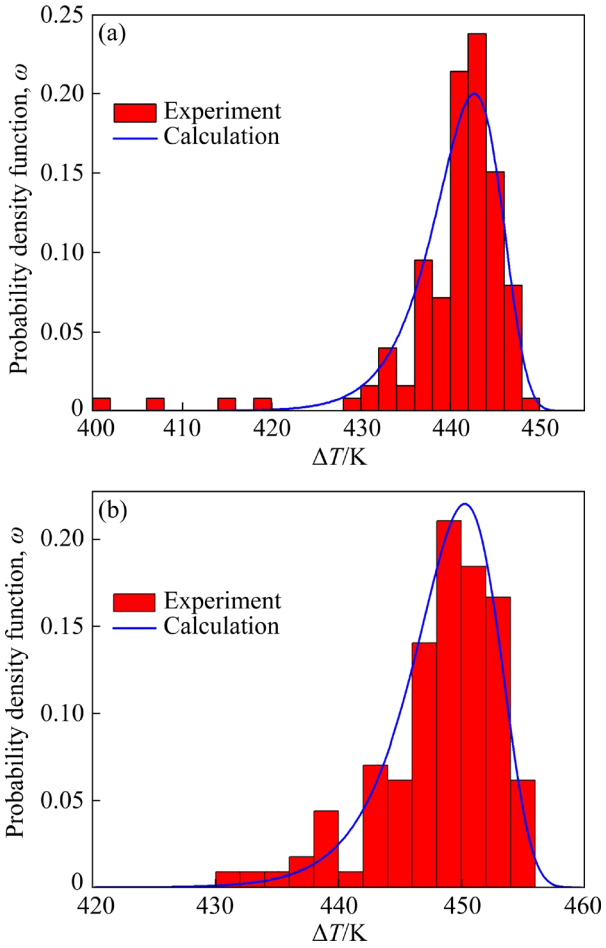

Fig. 8 Undercooling distribution of niobium samples cooled by natural radiation with different purities: (a) 99.7%; (b) 99.95%

mainly concentrated at 439−455 K, and the most probable nucleation undercooling is 450.3 K.

According to the classical nucleation theory, the nucleation rate function (I) of the sample material can be expressed by the following equation [38]:

$$I=K_{\mathrm{V}}\exp\left(-\frac{\Delta G^{*}}{k_{\mathrm{B}}T}\right) \tag{4}$$

where K_{V} is the pre-exponential factor; ΔG^{*} is the nucleation activation energy; k_{B} is the Boltzmann constant; T is the sample temperature.

The nucleation event in an electrostatic levitation device occurs under non-isothermal conditions. In the temperature range from T to $T+\delta T$, the probability density function ω is [39]

$$\omega(1,T+\delta T)=\delta T\frac{IV}{R_{\mathrm{C}}}\exp\left(\int_{T_{\mathrm{m}}}^{T}\frac{IV}{R_{\mathrm{C}}}\mathrm{d}T\right) \tag{5}$$

where V is the sample volume; R_{C} is the cooling rate of the sample, which is obtained from the cooling curve of the sample.

Assuming that the dependence of K_{V} on temperature is very weak, the cumulative distribution function (F) can be obtained from Eq. (5) [39]:

$$F=1-\exp\left(\frac{VK_{\mathrm{V}}}{R_{\mathrm{C}}\mathrm{d}\left(-\frac{\Delta G^{*}}{k_{\mathrm{B}}T}\right)/\mathrm{d}T}\exp\left(\frac{CT^{2}}{\Delta T^{2}}\right)\right) \tag{6}$$

$$\frac{\mathrm{d}\left(-\frac{\Delta G^{*}}{k_{\mathrm{B}}T}\right)}{\mathrm{d}T}=2C\frac{T\cdot\Delta T+T^{2}}{\Delta T^{3}} \tag{7}$$

According to Eqs. (6) and (7), the cumulative distribution function (F) can be simplified as

$$F=1-\exp\left(\frac{VK_{\mathrm{V}}\Delta T^{3}}{2CR_{\mathrm{C}}\left(\Delta T\cdot T+T^{2}\right)}\exp\left(\frac{CT^{2}}{\Delta T^{2}}\right)\right) \tag{8}$$

The values of F and R_{C} are obtained from the experimental data. According to the experimental results, the relationship between $\ln[-\ln(1-F)]$ and $T^{2}/\Delta T^{2}$ is shown in Fig. 9. The value of C can be obtained from the slope. The value of C is −1.869 and −2.151 for the sample with 99.7% purity and 99.95 purity. K_{V} and ΔG^{*} are calculated from the fitting curve at the most probable nucleation undercooling. In this work, for 99.7% Nb, K_{V} and ΔG^{*} values are $1.815\times10^{32}\,\mathrm{m^{-3}\cdot s^{-1}}$ and $55.30k_{\mathrm{B}}T$, respectively. And for Nb with 99.95% in purity, the K_{V} and ΔG^{*} values are $4.009\times10^{34}\,\mathrm{m^{-3}\cdot s^{-1}}$ and $60.71k_{\mathrm{B}}T$, respectively. The results illustrate that at the slightly higher purity, higher values of K_{V} and ΔG^{*} would be obtained. The relation curves between nucleation probability density function (ω) and undercooling are drawn in Fig. 8, which are consistent with the data of experimental undercooling distribution.

The calculated K_{V} and ΔG^{*} values in this work and other works are listed in Table 3. Figure 10 shows the statistics of the undercooling distribution of niobium with different purities under the electrostatic levitation condition in this work and other results.

Our results have shown that different experimental environments and methods result in

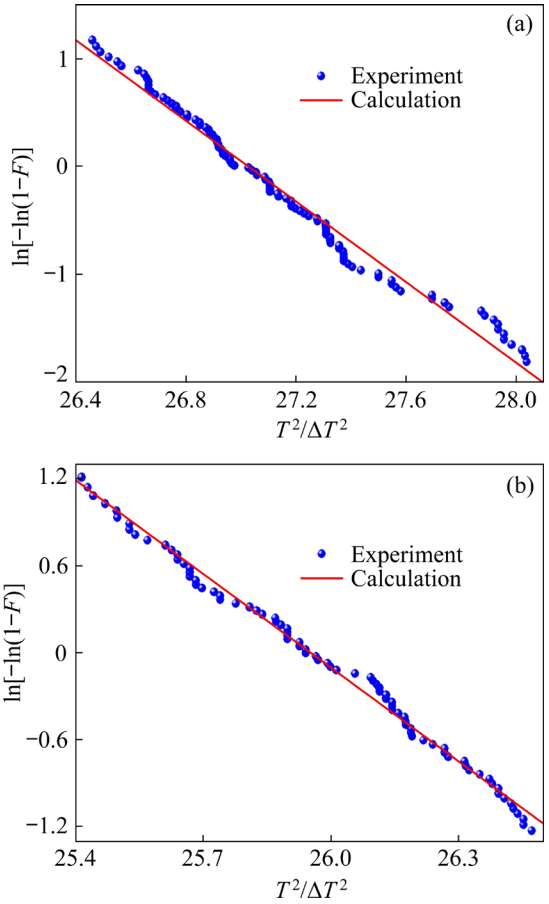

Fig. 9 Relationship between F and undercooling of Nb with different purities: (a) 99.7% Nb; (b) 99.95% Nb

different undercooling distributions. In this experiment, with a slight decrease in sample purity, the maximum probability of undercooling, K_V, and G^* value show a clear decrease, indicating that impurity has a significant influence on the undercooling ability and nucleation mechanism of liquid niobium.

3.5 Crystal/liquid interface free energy

In this section, the Gibbs free energy difference, critical nucleus radius, and solid/liquid interface free energy of liquid Nb are calculated according to the experimental data.

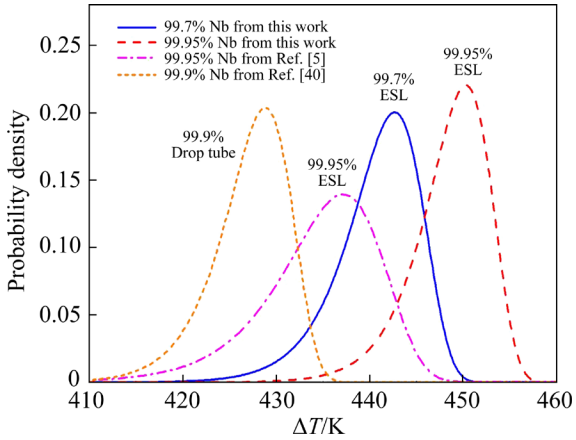

Fig. 10 Nucleation probability density versus undercooling ΔT of Nb with different purities and methods

ARBLASTER [41] measured that the solid-state specific heat capacity value of niobium at the melting point temperature is 44.39 $J \cdot mol^{-1} \cdot K^{-1}$. Combined with the experimental data, the change of Gibbs free energy difference with undercooling can be calculated by Eq. (9):

$$\Delta G_m = \Delta H_{LS} - T\Delta S_{LS} \quad (9)$$

Figure 11 shows the calculation of Gibb's free energy difference in this work and TURNBULL's model [42]. With the increase of undercooling, the deviations between the experiment and the model become larger. This indicates that the traditional estimation methods can only describe the solidification process under low undercooling conditions.

The relationship between the nucleation activation energy ΔG^* and the Gibbs free energy difference ΔG_m is as follows [43]:

$$\Delta G^* = \frac{16\pi\sigma^3}{3\Delta G_m^2} \quad (10)$$

where σ is the solid/liquid interface free energy.

The growth process of the critical nucleus is a spontaneous thermodynamic process, and its radius (r_c) is

Table 3 Maximum probability undercooling, K_V value and ΔG^* value of niobium with different purities

Source	Purity/%	Method	Maximum probability undercooling/K	$K_V/(m^{-3} \cdot s^{-1})$	$\Delta G^*/(k_B T)$
MORTON et al [40]	99.9	Drop tube	428.8	10^{31}	73.2
YANG et al [5]	99.95	ESL	438	1.02×10^{30}	47.73
This work	99.7	ESL	442.7	1.815×10^{32}	55.3
	99.95	ESL	450.3	4.009×10^{34}	60.7

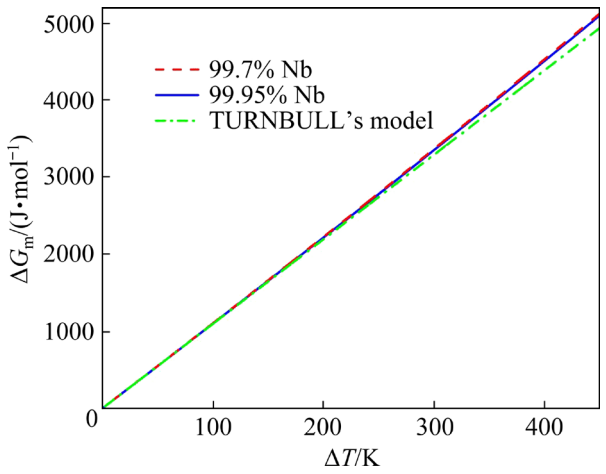

Fig. 11 Gibbs free energy difference versus undercooling

$$r_c=\frac{2\sigma}{\Delta G_m} \tag{11}$$

α is the configuration entropy difference between crystal and liquid at the interface, which is calculated by the following formula [44]:

$$\alpha=\frac{(N_A V_m^2)^{1/3}}{\Delta H_m}\sigma \tag{12}$$

where N_A is Avogadro constant; V_m is the molar volume.

Combined with the experimental data, according to Eqs. (10)−(12), solid/liquid interface free energy, critical nucleus radius, and α value of niobium with different purity can be calculated. In this work, for Nb with 99.7% purity, σ, r_c, and α values are 0.271 J/m^2, 1.245 nm, and 0.387, respectively. For Nb with 99.95% purity, σ, r_c, and α values are 0.283 J/m^2, 1.274 nm, and 0.407, respectively.

YANG et al [5], KANG et al [9], and MORTON et al [40] conducted several undercooling experiments on metal niobium by electrostatic levitation and drop tube method. According to their measurement results of nucleation activation energy of niobium with different purities, the solid/liquid interface free energy of Nb can be calculated. Table 4 lists r_c, σ, and α values calculated in this work and others. The results in this work show that at the higher Nb purity, the values of solid/liquid interface free energy, critical nucleus radius, and the configuration entropy difference between crystal and liquid at the interface are all higher than those at the lower Nb purity. Compared to the research results of previous works, our results have a slight difference due to different measurement methods.

3.6 Rapid dendrite growth under deep undercooling

The undercooled degree has great influence on the dendrite growth velocity of materials. In general, the greater the undercooling is, the faster the dendrite growth is. The LKT/BCT model can effectively describe the dendrite growth process and is used to investigate the relationship among undercooling, dendrite growth velocity, and dendrite tip radius [45].

In the LKT/BCT model, the total undercooling consists of four sub-undercooling degrees [46]:

$$\Delta T=\Delta T_c+\Delta T_t+\Delta T_k+\Delta T_r \tag{13}$$

where ΔT_c is component undercooling; ΔT_t is thermal undercooling; ΔT_k is dynamic undercooling; ΔT_r is the curvature undercooling of the dendrite tip. In this work, because the purity of Nb is 99.7% and 99.95%, the effect of component undercooling can be ignored.

To find the unique solution to Eq. (13), a stability equation is needed:

$$R=\frac{\Gamma/\sigma^*}{\left(\Delta H_m/C_p\right)P_t\xi_t} \tag{14}$$

Table 4 Solid/liquid interface free energy, critical nucleus radius, and α value of niobium with different purities

Author	Purity/%	ΔG_m/(J·m^{-3})	r_c/nm	σ/(J·m^{-2})	α	Method
This work	99.7	4.344×10^8	1.245	0.271	0.387	ESL
	99.95	4.445×10^8	1.274	0.283	0.407	ESL
YANG et al [5]	99.95	4.295×10^8	1.191	0.256	0.368	ESL
KANG et al [9]	99.95	5.565×10^8	1.150	0.320	0.478	ESL
MORTON et al [40]	99.9	4.200×10^8	1.386	0.291	0.418	Drop tube

where R is the dendrite tip radius; σ^* is the stability constant; Γ is the Gibbs−Thomson coefficient; P_t is the thermal Péclet number; ξ_t is the stability parameter related to the Péclet number.

An appropriate selection criterion is indispensable to determine the value of σ^* and is more essential to the analysis of the dendrite growth velocity in the procedure of electrostatic levitation rapid solidification. Marginal stability (MS) theory is a classical selection criterion for free dendrite growth which believes that the stability constant can be approximately assumed to be $1/(4\pi^2)$ [47]. However, the solvability condition (SC) theory is an improved selection criterion for non-isothermal and non-equilibrium solidification conditions by considering the effect of the anisotropy of surface energy [48]. Herein, the combination of electrostatic levitation and laser heating containerless method can provide deeper undercooling and obtain metastable materials, which is a non-isothermal procedure, and thus the anisotropy of surface energy is an important factor that should not be neglected in dendrite growing of rapid solidification (Table 5).

Combined with the physical parameters of Nb, the relationship between the undercooling and the dendrite growth velocity by LKT/BCT model can be obtained. The physical parameters required in the calculation are itemized in Table 6.

The maximum dendrite growth velocity of Nb in the undercooled state can reach dozens of meters per second. In order to observe the solid/liquid interface migration of the sample during solidification and infer its dendrite growth velocity, the sample is photographed at 2×10^5 fps with an ultra-high-speed camera (i-speed508). As shown in Fig. 12, the dark part is a liquid region and the bright part is a solid region. It can be seen that a nucleation point is formed on the sample surface, and then the crystal nucleus grows rapidly.

Table 5 Selection criterion for stable regime of growing dendritic tip

Parameter	Function	Solvability condition theory [48]	Marginal stability theory [47]
Stability constant	σ^*	$\sigma_0\beta^{7/4}$	$1/(4\pi^2)$
Stability parameter related to Péclet number	$\xi_t(P_t)$	$\dfrac{1}{(1+a_1\sqrt{\beta}P_t)^2}$	$1-\dfrac{1}{\left(1+\dfrac{1}{\sigma^* P_t^2}\right)^{1/2}}$

a_1 is a constant [48]; β is the surface energy stiffness

Table 6 Physical parameters of pure Nb used in LKT/BCT calculations

Parameter	Value	Source
Enthalpy of fusion, $\Delta H_m/(J\cdot mol^{-1})$	30013.72	This work
Specific heat capacity, $C_p/(J\cdot mol^{-1}\cdot K^{-1})$	40.55	This work
Gibbs−Thomson coefficient, $\Gamma/(K\cdot m)$	5.69×10^{-7}	GALE and TOTEMEIER [49]
Thermal diffusion coefficient/$(m^2\cdot s^{-1})$	2.3×10^{-5}	GALE and TOTEMEIER [49]
Sound speed, $V_0/(m\cdot s^{-1})$	2000	GALE and TOTEMEIER [49]
Surface energy stiffness, β	0.18	ALEXANDROV et al [48]
Stability parameter, σ_0	0.025	Fitting

The photos of solid/liquid interface migration with different undercoolings are recorded by an ultra-high-speed camera, and then the velocity could be derived by the time and position of the migration images through an image processing approach. The velocity is fitted as Eq. (15). Figure 13 demonstrates the relationship between the dendrite growth velocity v (m/s) and the undercooling ΔT (K) of niobium.

$$\begin{cases} v = 1.06\times10^{-8}\Delta T^{3.61} (99.7\%\ \text{Nb}) \\ v = 9.31\times10^{-10}\Delta T^{4.01} (99.95\%\ \text{Nb}) \end{cases} \tag{15}$$

The dendrite growth velocity of pure Nb demonstrates a power function with undercooling. YANG et al [5] measured the dendrite growth velocity of niobium by electrostatic levitation technology and the speed at undercooling of 454 K was about 41 m/s. In this work, the measurement results are 41.4 m/s (99.7% Nb) and 42.1 m/s (99.95% Nb) at the undercooling of 454 K, which are close to that of YANG et al [5]. By substantially considering the effect of anisotropy of surface energy, the deviation of the solvability condition theory prediction result is much smaller than that of the marginal stability theory prediction result. Meanwhile, our research results show better consistency compared to the results of YANG et al [5]. This indicates that anisotropy of surface energy plays a significant role in the electrostatic

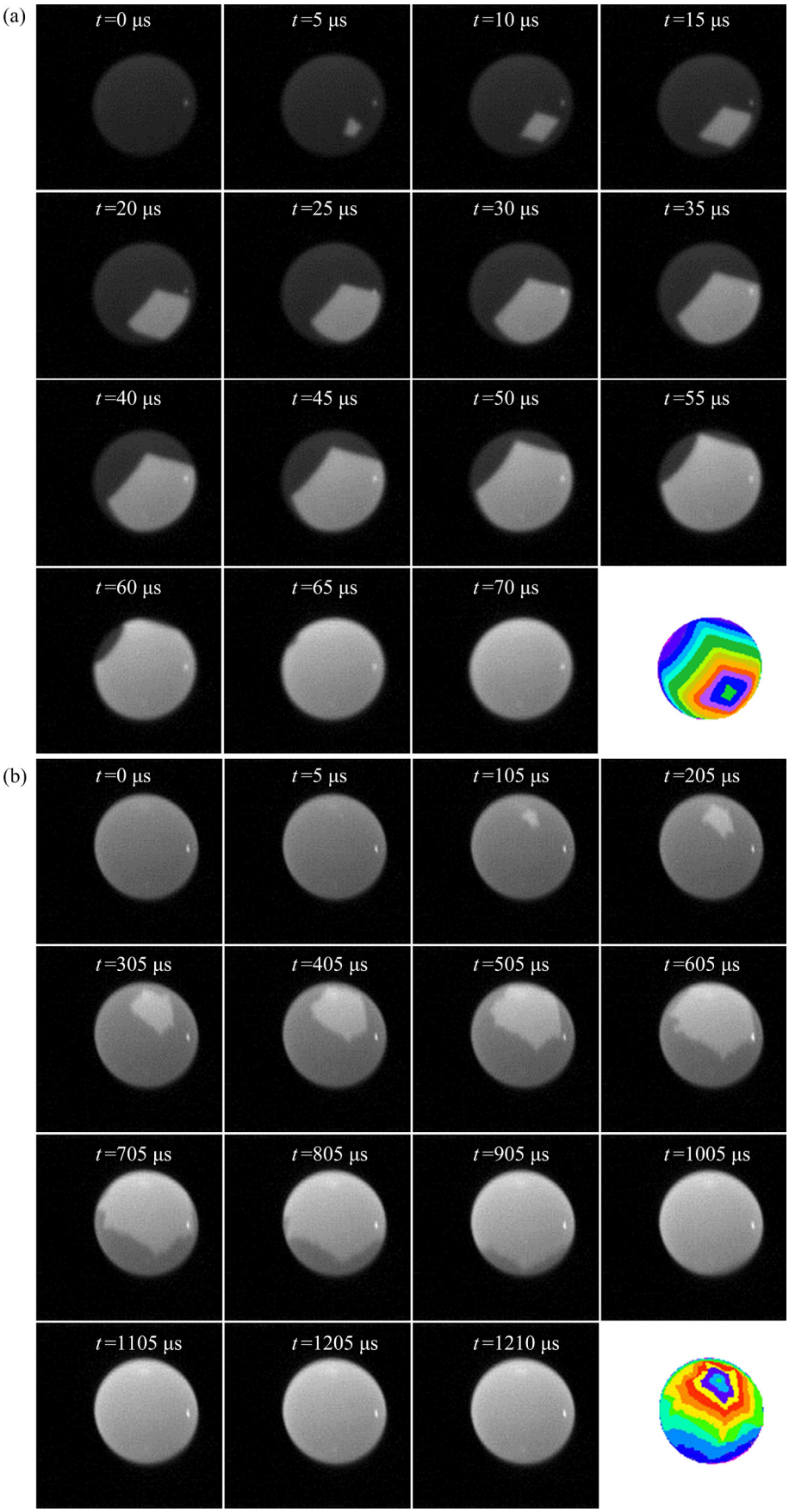

Fig. 12 Solid/liquid interface migration during recalescence of undercooled Nb (shooting rate is 2×10^5 fps): (a) 99.7% Nb with undercooling of 447.3 K; (b) 99.95% Nb with undercooling of 153.3 K

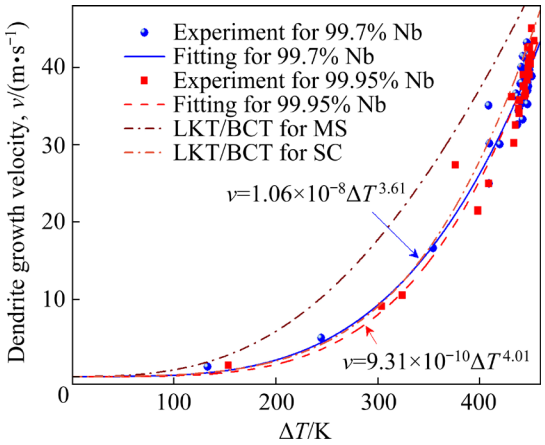

Fig. 13 Dendritic growth velocity versus undercooling of Nb

levitation rapid solidification that should be taken into account in the analysis of dendrite growth velocity. The impurity can be regarded as a certain type of additive, and our results also give another proof of additive technology [50,51].

4 Conclusions

(1) According to the experimental data, the thermophysical properties related to the nucleation and solidification procedures are calculated, including the hyper cooling limit, the liquid-state specific heat capacity, and the fusion enthalpy.

(2) The relationship between the undercooled degree and the cooling rate before nucleation is studied. The measurement results have illustrated that the smaller cooling rate corresponds to the larger undercooling, which provides the possibility to control the undercooled degree by controlling the cooling rate of the sample.

(3) Through the statistical analysis of the undercooling distribution of the Nb samples with different purities, the most probable nucleation undercooling, the pre-exponential factor, the nucleation activation energy, the solid/liquid interface free energy, and the critical nucleus radius are obtained. The impurity can be regarded as a type of additive that plays an important role in the heterogeneous nucleation and dendritic growth procedures of Nb. It can be assumed that a minor increase in additive concentration significantly changes the undercooling distribution and nucleation behavior.

(4) The solid/liquid interface migration images of the sample surface during the solidification process were captured by an ultra-high-speed camera, and the growth rate of the dendrite was estimated. The experimental results show that the dendrite growth velocity has a powerful relationship with undercooling. At the undercooling of 454 K, the dendrite growth velocity is about 42.1 m/s. The effect of anisotropy of surface energy is considered in the analysis of dendrite growth velocity and shows great consistency with our experiment results.

CRediT authorship contribution statement

Yan-qiu WANG: Conceptualization, Methodology, Original draft preparation, Writing − Review and editing; **Fu ZHENG:** Software; **Xiao-xiao LU:** Software; **Zhi-bin SUN:** Conceptualization, Project administration, Funding acquisition.

Declaration of competing interest

The authors declare that they have no known competing financial interests or personal relationships that could have appeared to influence the work reported in this paper.

Acknowledgments

This work was supported by the Scientific Instrument Developing Project of the Chinese Academy of Sciences (No. YJKYYQ20190008), the Strategic Pioneer Program on Space Science, Chinese Academy of Sciences (No. XDA15013600), and the Youth Innovation Promotion Association of the Chinese Academy of Sciences (Nos. 2013105, Y201728).

References

[1] LI Sheng, LIU Feng, YANG Wei. Comparison of dendrite and dispersive structure in rapidly solidified Cu−Co immiscible alloy with different heat flow modes [J]. Transactions of Nonferrous Metals Society of China, 2017, 27: 227−233.

[2] XIAO Rui-lin, RUAN Ying, LIN Mao-jie, QIN Jing-yu, LI Hui, HU Liang, WEI Bing-bo. Metastable liquid properties and rapid crystal growth of Ti−Ni−Al alloy investigated by electrostatic levitation and molecular dynamics simulation [J]. Science China: Technological Sciences, 2021, 64: 2200−2210.

[3] YAN Xue-wei, GUO Xiong, LIU Yan-ling, GONG Xiu-fang, XU Qing-yan, LIU Bai-cheng. Numerical simulation of dendrite growth in Ni-based superalloy casting during directional solidification process [J]. Transactions of Nonferrous Metals Society of China, 2019, 29: 338−348.

[4] SUN Yu, PANG Shao-ping, LIU Xue-ran, YANG Zi-run,

SUN Guo-xiong. Nucleation and growth of eutectic cell in hypoeutectic Al−Si alloy [J]. Transactions of Nonferrous Metals Society of China, 2011, 21: 2186−2191.

[5] YANG S J, HU L, WANG L, WEI B. Heterogeneous nucleation and dendritic growth within undercooled liquid niobium under electrostatic levitation condition [J]. Chemical Physics Letters, 2017, 684: 316−320.

[6] HERLACH D M, BINDER S, GALENKO P, GEGNER J, HOLLAND-MORITZ D, KLEIN S, KOLBE M, VOLKMANN M. Containerless undercooled melts: Ordering, nucleation, and dendrite growth [J]. Metallurgical and Materials Transactions A, 2015, 46: 4921−4936.

[7] LIU Li, MA Xiao-li, HUANG Qi-sen, LI Jin-fu, CHENG Xian-hua, ZHOU Yao-he. Solidification process and microstructure evolution of bulk undercooled Co−Sn alloys [J]. Transactions of Nonferrous Metals Society of China, 2013, 23: 289−293.

[8] YU J, PARADIS P F, ISHIKAWA T, YODA S. Dielectric constant of barium titanate synthesized by containerless processing [J]. MRS Online Proceedings Library, 2004, 848: 1−6.

[9] KANG D H, JEON S, YOO H, ISHIKAWA T, OKADA J T, PARADIS P F, LEE G W. Nanosized nucleus-supercooled liquid interfacial free energy and thermophysical properties of early and late transition liquid metals [J]. Crystal Growth & Design, 2014, 14: 1103−1109.

[10] LEE G W, CHO Y C, LEE B, KELTON K F. Interfacial free energy and medium range order: Proof of an inverse of Frank's hypothesis [J]. Physical Review B, 2017, 95: 054202.

[11] ISHIKAWA T, KOYAMA C, NAKATA Y, WATANABE Y, PARADIS P F. Spectral emissivity, hemispherical total emissivity, and constant pressure heat capacity of liquid vanadium measured by an electrostatic levitator [J]. The Journal of Chemical Thermodynamics, 2021, 163: 106598.

[12] HERLACH D, MATSON D. Solidification of containerless undercooled melts [M]. Wiley-VCH Verlag GmbH & Co. KGaA: 2012: 07−18.

[13] KATO K, MASUNO A, INOUE H. Containerless solidification of undercooled SrO−Al_2O_3 binary melts [J]. Physical Chemistry Chemical Physics, 2015, 17: 6495−6500.

[14] MA Bing-qian, LI Jian-qiang, XU Zhe, PENG Zhi-jian. Fe-shell/Cu-core encapsulated metallic phase change materials prepared by aerodynamic levitation method [J]. Applied Energy, 2014, 132: 568−574.

[15] SHA S, CHANG J, XU S S, YAN P X, WEI B. Microstructural evolution and magnetic property of rapidly solidified Co62Mo38 hypereutectic alloy [J]. Materials Letters, 2021, 291: 129574.

[16] ROGERS J R, HYERS R W, RATHZ T, SAVAGE L, ROBINSON M B. Thermophysical property measurement and materials research in the NASA/MSFC electrostatic levitator [J]. AIP Conference Proceedings, 2001, 552: 332−332.

[17] WANG Fei-long, DAI Bin, LIU Xue-feng, SUN Yi-ning, SUN Zhi-bin, YU Qiang, ZHAI Guang-jie. Containerless heating process of a deeply undercooled metal droplet by electrostatic levitation [J]. Chinese Physics Letters, 2015, 32: 114101.

[18] RHIM W K, CHUNG S K, DANIEL B, MAN K F, GUTT G, RULISON A, SPJUT R E. An electrostatic levitator for high temperature containerless materials processing in 1-g [J]. Review of Scientific Instruments, 1993, 64: 2961−2970.

[19] PARADIS P F, RHIM W K. Thermophysical properties of zirconium at high temperature [J]. Journal of Materials Research, 1999, 14: 3713−3719.

[20] HORNFECK W, KOBOLD R, KOLBE M, CONRAD M, HERLACH D. Quasicrystal nucleation and Z module twin growth in an intermetallic glass-forming system [J]. Nature Communications, 2018, 9: 1−6.

[21] LEE G W, JEON S, LEE, PARK C, KANG D H. Crystal−liquid interfacial free energy and thermophysical properties of pure liquid Ti using electrostatic levitation: Hypercooling limit, specific heat, total hemispherical emissivity, density, and interfacial free energy [J]. Journal of Chemical Thermodynamics, 2013, 63: 1−6.

[22] ZOU P F, WANG H P, ZHENG C H, HU L, CHANG J, WEI B. Electrostatic levitation processing and microscopic hardness property of hyperperitectic Ti60Ni40 alloy [J]. Intermetallics, 2021, 130: 106934.

[23] XUE Shu-qi, DONG Wen-bo, CHEN Dong-yang, GUO Qing-yuan, HE Huan, YU Jian-ding. Analysis of electrostatic levitation control system and oscillation method for material properties measurement [J]. Review of Scientific Instruments, 2021, 92: 065111.

[24] ZHONG Qiu, YANG Li-ping, LI Hui-dong, TAO Ye, WANG Wen-bin, XU Zi-jun, LUO Cai-yun. A new 3D reconstruction method for the density measurement of ellipsoid levitated droplets with containerless technique [J]. Journal of Molecular Liquids, 2020, 316: 113345.

[25] ISHIKAWA T, KOYAMA C, NAKATA Y, WATANABE Y, PARADIS P F. Spectral emissivity and constant pressure heat capacity of liquid titanium measured by an electrostatic levitator [J]. Journal of Chemical Thermodynamics, 2019, 131: 557−562.

[26] PARADIS P F, ISHIKAWA T, SAITA Y, YODA S. Containerless property measurements of liquid palladium [J]. International Journal of Thermophysics, 2004, 25: 1905−1912.

[27] SUNG Y S, TAKEYA H, TOGANO K. Containerless solidification of Si, Zr, Nb, and Mo by electrostatic levitation [J]. Review of Scientific Instruments, 2001, 72: 4419−4423.

[28] SANSOUCIE M P, ROGERS J R, KUMAR V, KODRIGUEZ K, XIAO X, MATSON D M. Effects of environmental oxygen content and dissolved oxygen on the surface tension and viscosity of liquid nickel [J]. International Journal of Thermophysics, 2016, 37: 1−11.

[29] ISHIKAWA T, PARADIS P F. Thermophysical properties of molten refractory metals measured by an electrostatic levitator [J]. Journal of Electronic Materials, 2005, 34: 1526−1532.

[30] PARADIS P F, ISHIKAWA T, KOIKE N, WATANABE Y. Physical properties of liquid terbium measured by levitation techniques [J]. Journal of Rare Earths, 2007, 25: 665−669.

[31] HU L, WANG W L, YANG S J, LI L H, CENG D L, WANG L, WEI B. Dendrite growth within supercooled liquid tungsten and tungsten-tantalum isomorphous alloys [J]. Journal of Applied Physics, 2017, 121: 085901.

[32] PARADIS P F, ISHIKAWA T, LEE G W, MORITZ D H, BRILLO J, RHIM W K, OKADA J T. Materials properties measurements and particle beam interactions studies using electrostatic levitation [J]. Materials Science and

Engineering R−Reports, 2014, 76: 1−53.
[33] ISHIKAWA T, PARADIS P F, YODA S. New sample levitation initiation and imaging techniques for the processing of refractory metals with an electrostatic levitator furnace [J]. Review of Scientific Instruments, 2001, 72: 2490−2495.
[34] WILTHAN B, CAGRAN C, POTTLACHER G. Combined DSC and pulse-heating measurements of electrical resistivity and enthalpy of tungsten, niobium, and titanium [J]. International Journal of Thermophysics, 2005, 26: 1017−1029.
[35] PARADIS P F, ISHIKAWA T, YODA S. Non-contact measurements of thermophysical properties of niobium at high temperature [J]. Journal of Materials Science, 2001, 36: 5125−5130.
[36] SAKATA K, WATANABE Y, OKADA J T, KUMAR M V, PARADIS P F, ISHIKAWA T. FT-IR emissivity measurements of Nb melt using an electrostatic levitation furnace [J]. Journal of Chemical Thermodynamics, 2015, 91: 116−120.
[37] BETZ G, FRONHBERG M G. Enthalpy measurements on solid and liquid niobium by means of levitation calorimetry [J]. International Journal of Materials Research, 1980, 71: 451−455.
[38] TURNBULL D. Under what conditions can a glass be formed? [J]. Contemporary Physics, 1969, 10: 473−488.
[39] KLEIN S, HOLLAND-MORITZ D, HERLACH D M. Crystal nucleation in undercooled liquid zirconium [J]. Physical Review B, 2009, 80: 212202.
[40] MORTON C W, HOFMEISTER W H, BAYUZICK R J, ROBINSON M B. A statistical approach to understanding nucleation phenomena [J]. Materials Science and Engineering A, 1994, 178: 209−215.
[41] ARBLASTER J W. The thermodynamic properties of niobium [J]. Journal of Phase Equilibria and Diffusion, 2017, 38: 707−722.
[42] TURNBULL D J. Formation of crystal nuclei in liquid metals [J]. Journal of Applied Physics, 1950, 21: 1022−1028.
[43] VINET B, MAGNUSSON L, FREDRIKSSON H, DESRE P J. Correlations between surface and interface energies with respect to crystal nucleation [J]. Journal of Colloid and Interface Science, 2002, 255: 363−374.
[44] KANG D H, ZHANG H, YOO H, LEE H H, LEE S, LEE G W, LOU H, WANG X D, CAO Q P, ZHANG D X, JIANG J Z. Interfacial free energy controlling glass-forming ability of Cu−Zr alloys [J]. Scientific Reports, 2014, 4: 5167.
[45] CHAO Y, GAO J. Modeling of free eutectic growth and competitive solidification in undercooled near-eutectic alloys based on in situ measurements [J]. Journal of Materials Science, 2015, 50: 268−278.
[46] LU Yi-ping, LIU Feng, YANG Gen-cang, WANG Hai-peng, ZHOU Yao-he. Grain refinement in solidification of highly undercooled eutectic Ni−Si alloy [J]. Materials Letters, 2007, 61: 987−990.
[47] GALENKO P K, DANILOV D A. Linear morphological stability analysis for the solid-liquid interface in rapid solidification of a binary system [J]. Physical Review E, 2004, 69: 051608.
[48] ALEXANDROV D V, DANILOV D A, GALENKO P K. Selection criterion of a stable dendrite growth in rapid solidification [J]. International Journal of Heat and Mass Transfer, 2016, 101: 789−799.
[49] GALE W F, TOTEMEIER T C. Smithells metals reference book [M]. Oxford: Butterworth-Heinemann, 2004: 13−14.
[50] FOLEY B J, GIRARD J, SORENSON B A, CHEN A Z, NIEZGODA J S, ALPERT M R, HARPER A F, SMILGIES D M, CLANCY P, SAIDI W A, CHOI J J. Controlling nucleation, growth, and orientation of metal halide perovskite thin films with rationally selected additives [J]. Journal of Materials Chemistry A, 2017, 5: 113−123.
[51] MATVEEV M, PROMAKHOV V, SCHULTZ N, VOROZHTSOV A. Synthesis of metal matrix composites based on Cr_xNi_y-TiN for additive technology [J]. Materials, 2021, 14: 1−11.

静电悬浮下铌异质形核及枝晶生长

王艳秋[1,2]，郑 福[1]，陆潇晓[1,2]，孙志斌[1,2]

1. 中国科学院 国家空间科学中心，北京 100190；
2. 中国科学院大学，北京 101499

摘 要：采用无容器静电悬浮实验技术，对纯度 99.7%和 99.95%铌材料的过冷程度和形核凝固机制进行了系统研究。通过经典形核理论分析测量和计算得到材料样品在形核和凝固过程的热物理参数和热动力学参数。实验结果统计分析表明：铌样品的最大过冷度为 455.7 K，临界过冷度约为 739 K。系统分析并计算得到铌样品最大概率形核过冷度、指前系数、成核活化能、固液界面自由能和关键晶核尺寸。样品的枝晶生长速度与过冷度呈幂函数关系，在过冷度 454 K 时，枝晶生长速度达到 42.1 m/s。考虑非等温条件下界面能的各向异性对自由枝晶生长的影响，理论预测结果与实验获得实验结果一致。

关键词：液态铌；异质形核；枝晶生长；形核凝固机制；无容器静电悬浮

(Edited by Bing YANG)